J. Basic. Appl. Sci. Res., 3(2s)689-697, 2013

ISSN 2090-4304
Journal of Basic and Applied Scientific Research
www.textroad.com

Modeling energy performance of a home heating system, with three config / Photo Vltayy into building

E. Shamshiry*, M. Rajaee

University of Shariati, Tehran

Received: June 10 2013
Accepted: July 10 2013

ABSTRACT

In this paper we research results and practical In this paper, we investigate theoretical and practical results on the energy performance of our three different thermal / photovoltaic into building Vltayy Open to air heating used to provide heat is recovered again. First configure the basic mode Not Working BIPV glazing with air flow at the bottom the first and second configuration with a 1.5-meter vertical work-glazed air collector PV panels glazed and third configuration is working. The proposed model of the experimental data to a first configuration uses solar test home. The relationship between air temperature and exhaust systems for BIPV / T, which Function of solar radiation and air flow rate in the PV cavity can be also applied to decisions about Fan Control The outlet air temperature is appropriate. The first configuration of the pre-heated air and HVAC systems for heating domestic hot water (DHW) is more appropriate. In order to get more air out of the cavity temperatures used in PV and DHW, can be used to configure the second and third. Second, even in the winter time can be configured using the outlet air temperature was too high and the thermal efficiency somewhat raised this system could also be used to heat sources embedded in the soil matrix. Finally, the third configuration by reducing electricity generation PV panels will lead to a dramatic increase in temperature.

KEYWORD: Building integrated photovoltaics, water heat exchanger-air heating / photovoltaic into building, domestic hot water, solar air collector.

INTRODUCTION

Vltayy photovoltaic panels mounted on the building of new technologies in sustainable building design. The panels can provide heat and electricity for the home. If heat and electricity through photovoltaic systems within the building Vltayy (BIPV) is provided, BIPV system to heat or BIPV / T system is modular and PV / T call. A theoretical study on PV systems installed in the entrance to the house was air the impact of various design parameters on the electrical function - heating system review [1]. Simulation results connecting a collection of PV / T water on the wall of a water tank, Rate volumetric efficiency solar cell density factor Venice water system in order to get the desired energy output determined. Finally Bakker [2] that the ceiling panel PV / T heat pump under the ground were also examined. In this paper we investigate its action on the energy performance of three different roof BIPV / T that are working to open our presents.
Solar House Concordia [5], which can be seen in Figure 1, is used to illustrate the first configurations. The original model was designed with limited ceiling height and slope of the roof, the more energy you will get from the sun.

Figure 1. Picture of the Solar House Concordia.

2. The model developed

2.1 Introduction

Solar home design usually designed with a variety of challenges to face. PV panels must be carefully and correctly set up the solar maximum occurs In addition, costs are reduced as much as possible. Some of the most important problems

***Corresponding Author:** E. Shamshiry, University of shariati, Tehran. Email: elahe.shamshiry33@yahoo.com

facing the system design BIPV / T include how much electricity can be achieved Or how much heat can be reused, Or what kind of configuration BIPV / T roof, will show the best performance? In this paper, we plan on using recycled heat Tuesday configuration BIPV / T system using HV air and water heat exchanger - air DHW tank connected to a focus. The next section describes the methodology used more., In this paper we also considered relations for heat transfer coefficients of impulse flows, natural convection channels for the transmission line and use.

2.2 System Configuration

In our studies we plan Tuesday configured systems BIPV / T Open related HVAC components to consider.

First configure the basic mode Not Working BIPV glazing with air flow in the lower part is shown in Figure 2. The second configuration is the first alternative configuration is shown in Figure 3. Finally, the third configuration is shown in Figure 4. In all configurations, including 40 panel PV system PV7kW BP4175 crystal embedded into the roof of the south building, which contained a 4 cm cavity in which the pace air is circulated by a fan.

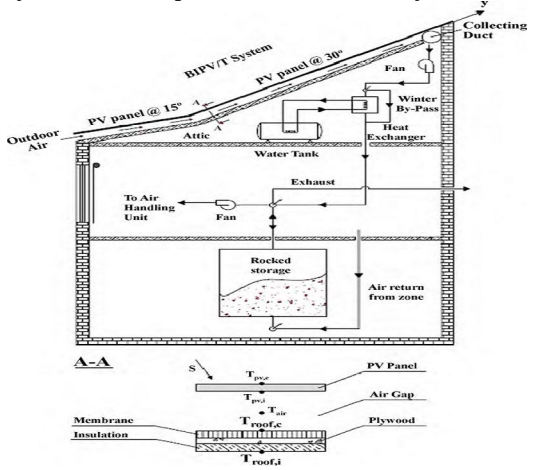

Fig 2. First configure the system, BIPV / T do not mucilage.

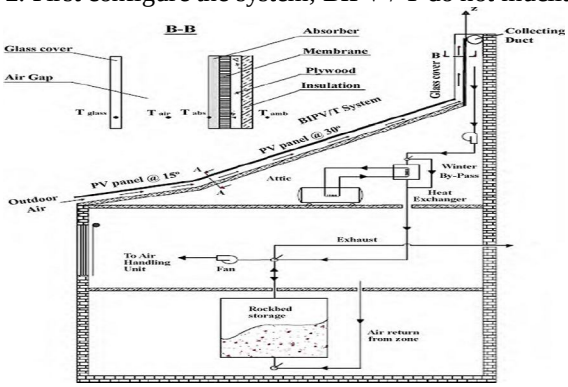

Fig 3. The second configuration system, BIPV / T glaze work with SAC.

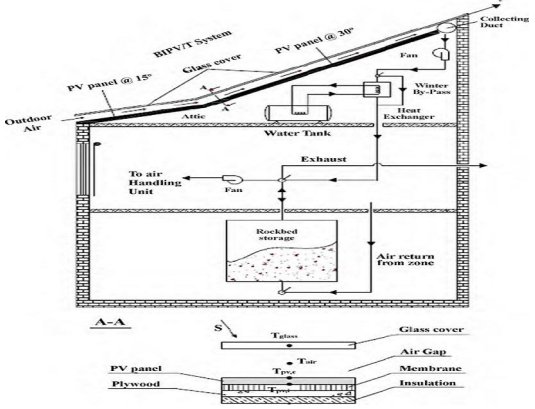

Fig 4. The third configuration system, BIPV / T glazing work.

The roof is composed of two parts - the first part of a 15-degree slope and is connected to the second part of the slope is 30 degrees. Environment where there is an urgent need for heating, Outside air by heat recovery systems, BIPV / T air handling unit is heated and is transferred to the heating process is excessive.

2.3 Model BIPV / T

For three tuning systems BIPV / T A mathematical model has been designed and implemented in MathCad 2001i. General assumptions in these simulations are one-dimensional heat transfer, the surface temperature of the PV channels per sector, not leaking air from the cavity PV, Same solar radiation on the outer surface, air-linear changes in BIPV / T for Short distances, equal CHTC values for the upper and lower surfaces of hollow PV and PV modules operate at the maximum power in the best condition possible. Motilo models were evaluated based on PV PV model proposed amendment with a diode [3]. His model Temperature dependence of short circuit current and open circuit voltage using empirical coefficients are determined to identify the manufacturers. Short circuit current, open circuit voltage and maximum power output of the following relationships are obtained:

$$I_{sc} = I_{sc,ref}\frac{\tau^*_{glass}\cdot S}{S_{ref}}[1+\alpha(T_{pv}-25\,^\circ\mathrm{C})] \quad (1)$$

$$V_{oc} = V_{oc,ref}[1-\gamma(T_{pv}-25\,^\circ\mathrm{C})\cdot\max\left(1+\beta\ln\left(\frac{\tau^*_{glass}\cdot S}{S_{ref}}\right)\right) \quad (2)$$

$$P_{el} = I_{mp,ref}\cdot V_{mp,ref}\left(\frac{I_{sc}\cdot V_{oc}}{I_{sc,ref}\cdot V_{oc,ref}}\right)\cdot m \quad (3)$$

Where * refers to the third configuration, Sref = 1000 W/m2 irradiance at standard test conditions, α the temperature coefficient Isc, β and γ the coefficient temperature coefficient of Voc Voc radiation is dimensionless. The system BIPV / T do not mucilage, the first configuration is shown in Figure 2, and the energy balance equations are expressed as follows:

External junction PV

$$U_0\cdot(T_{pv,e}-T_0)+U_{pv}\cdot(T_{pv,e}-T_{pv,i})+P_{el}=\alpha_{pv}\cdot S\cdot A_{pv} \quad (4)$$

Internal junction PV

$$U_{pv}\cdot(T_{pv,i}-T_{pv,e})+U_{h_1}\cdot(T_{pv,i}-T_{air})=U_{rad}\cdot(T_{roof,e}-T_{pv,i}) \quad (5)$$

Ceiling junction external

$$U_{rad}\cdot(T_{roof,e}-T_{pv,i})+U_{h2}\cdot(T_{roof,e}-T_{air}) = U_{roof}\cdot(T_{roof,i}-T_{roof,e}) \quad (6)$$

Ceiling junction

$$U_{roof}\cdot(T_{roof,i}-T_{roof,e})=U_{attic}\cdot(T_{attic}-T_{roof,i}) \quad (7)$$

Enthalpy changes in the model equal to the energy transferred to the air in the control volume of air movement. Air energy balance are as follows:

$$W\cdot h_1(T_{pv,i}-T_{air})+W\cdot h_2(T_{roof,e}-T_{air})=\dot{m}_{air}\cdot c_{p,air}\cdot\frac{dT_{air}}{dy} \quad (8)$$

We have the solution:

$$T_{air}(y)=\exp\left[-\frac{(h_1+h_2)\cdot W\cdot y}{m_{air}\cdot c_{p,air}}\right]\cdot T_{in} + \left[1-\exp\left(-\frac{(h_1+h_2)\cdot W\cdot y}{m_{air}\cdot c_{p,air}}\right)\right]\cdot \times\left(\frac{h_1\cdot T_{pv,i}+h_2\cdot T_{roof,e}}{h_1+h_2}\right) \quad (9)$$

Where Tin is the inlet air temperature. Tin with temperatures in the first part of the surrounding environment. About the rest of the system, BIPV / T, the temperature of the previous section can be used as input to the current section. Average temperatures range from the integration of Tair y = 0 to y = l with the boundary condition that the temperature of the surrounding air temperature is achieved.

$$\overline{T_{air}}=\frac{1}{L}\int_0^L T_{air}(y)dy \quad (10)$$

The system BIPV / TSAC second configuration is shown in Figure 3 and equations to calculate the temperature at the 11-13 junction with the previous algorithm is used. Absorption values, conductivity 0.04 W / mK, thickness 0.025 m and 0.95 are assumed to be absorbed.

Glass barrier junction

$$(T_{glass} - T_0) \cdot U_0 + (T_{glass} - T_{air}) \cdot U_{h_i} + (T_{glass} - T_{abs,e}) \cdot U_{rad} = \alpha_{glass} \cdot S \cdot A_{sac} \quad (11)$$

Point absorber

$$(T_{abs,e} - T_{glass}) \cdot U_{rad} + (T_{abs,e} - T_{air}) \cdot U_{h_i} + (T_{abs,e} - T_{abs,i}) \cdot U_{abs} = \tau_{glass} \cdot \alpha_{abs} \cdot S \cdot A_{sac} \quad (12)$$

Energy balance climate

$$W \cdot h_1 (T_{glass} - T_{air}) + W \cdot h_2 (T_{abs,e} - T_{air}) = \dot{m}_{air} c_{p,air} \frac{dT_{air}}{dz} \quad (13)$$

System BIPV / T 11-13 glaze work on modeling relationships where the PV panels have been used as adsorbents. Heat collected (Qheat), reflected solar radiation (Srefl) and collecting electricity (Pel) can be formulated as follows:

$$Q_{heat} = \dot{m}_{air} \cdot c_{p,air} \cdot (T_{air,out} - T_o) \quad (14)$$

$$Q_{loss,top} = U_o \cdot (T_{pv,e} - T_o) \quad (15)$$

$$Q^*_{loss,top} = U_o \cdot (T_{glass,e} - T_o) \quad (16)$$

$$Q_{loss,bottom} = U_{roof} \cdot (T_{roof,e} - T_{roof,i}) \quad (17)$$

$$Q^*_{loss,bottom} = U_{pv} \cdot (T_{pv,e} - T_{pv,i}) \quad (18)$$

$$S_{refl} = (1 - \alpha_{pv}) \cdot A_{pv} \cdot S \cdot \tau^*_{glass} \quad (19)$$

Thus, the energy balance for the system, BIPV / T glazes and enamels do not work is expressed as follows:

$$A_{pv} \cdot S = Q_{heat} + Q_{loss,top} + Q_{loss,bottom} + P_{el} + S_{refl} \quad (20)$$

In order to compare the thermal performance of the optimized thermodynamic systems, heat removal factor (FR) is calculated as follows [8]:

$$F_R = \frac{\dot{m}_{air} \cdot c_{p,air}}{A_{pv} \cdot U_L} \left[1 - e^{-\left(\frac{A_{pv} U_L F'}{\dot{m}_{air} c_{p,air}} \right)} \right] \quad (21)$$

Where the efficiency factor (F ') is obtained from the following relationships:

$$F' = \frac{h_1 h_r + h_2 U_o + h_2 h_r + h_1 h_2}{(U_o + h_r + h_1) \cdot (U_{pv} + h_2 + h_r) - h_r^2} \quad (22)$$

$$U_L = \frac{(U_{pv} + U_o) \cdot (h_1 h_2 + h_1 h_r + h_2 h_r) + U_{pv} U_o (h_1 + h_2)}{h_1 h_r + h_2 U_o + h_2 h_r + h_1 h_2} \quad (23)$$

Radiative heat transfer coefficient hr is indicative and is calculated from the following equation:

$$h_r = \frac{4 \cdot \sigma \cdot (T_1^2 + T_2^2) \cdot (T_1 + T_2)}{1/\varepsilon_1 + 1/\varepsilon_2 - 1} \quad (24)$$

2.4 Heat exchange coefficient

In order to calculate the heat transfer coefficients have been introduced into the channel had several relationships. The coefficients with respect to the air flow in a variety of positions are available. The air flow can be natural, synthetic or a combination might also be linear, the impulse is.in this study it is assumed that the flow of air into the line input starts And due to go down that path unchanged.

Linear flow in the entrance and fully developed air movement when Re <2300 with 25 relationship is expressed as: [9]

$$h_c = \frac{k_{air}}{D_h} \left[1.86 \cdot \left(\frac{RePrD_h}{L} \right)^{1/3} \cdot \left(\frac{\mu}{\mu_s} \right)^{0.14} \right] \quad (25)$$

The equation for constant surface temperature Ts is valid for 0.48 <Pr <16700 and 0.0044 <μ / μs <9.75 is., For fully developed flow transfer coefficient is calculated as follows:

$$h_c = \frac{7.54 \cdot k_{air}}{D_h} \quad (26)$$

In relation to the transition zone 27 is used: [10]

$$h_c = \frac{k_{air}}{D_h}\left[0.116\cdot(Re^{2/3}-125)\cdot Pr^{1/3}\cdot\left(1+\left(\frac{D_h}{L}\right)^{2/3}\right)\cdot\left(\frac{\mu}{\mu_s}\right)^{0.14}\right] \quad (27)$$

Above equation for 2300 <Re <6000 is valid. In areas where air flow Momentum 6000 <Re <106 [11] the following formula is used:

$$h_c = \frac{k_{air}}{D_h}\left[\frac{\left(\frac{f}{8}\cdot(Re-1000)\cdot Pr\right)}{1+12.7\cdot\sqrt{\frac{f}{8}}\cdot(Pr^{2/3}-1)}\cdot\left(1+\left(\frac{D_h}{L}\right)^{2/3}\right)\right] \quad (28)$$

Where the friction factor is calculated as follows:

$$f=(1.82\log Re-1.64)^{-2}$$

The equation for 0 <Dh / l <1 and 0.6 <Pr <2000 is true.

2.5 Model Construction

A mathematical model to describe the thermal reaction of Home Solar PV panels do not mucilage embedded in the ceiling using MathCad 2001i software design and implementation has been The whole house as an area of 75 square meters is considered. Thermal network model to simulate the behavior of the heat transfer and thus applied to home heating network relationships obviously finite difference method as follows have been solved, [12]:

$$T(i,t+1)=\left(\frac{\Delta t}{C_i}\right)\left[q_i+\sum_j\frac{T(j,t)-T(i,t)}{R(i,j)}\right]+T(i,t) \quad (29)$$

Ci where i am attaching the heat capacity, R (I, j) thermal resistance between points i and j, and t is the current time. Absorbing heat from lights and appliances for an hour of time has been modeled. Penetration in the air chamber and the whole area is determined by equation 30:

$$U_{inf}=\frac{ACH\cdot Vol_z}{3600}\cdot\rho_{air}\cdot c_{p,air} \quad (30)$$

0.5 and penetration of air per hour is assumed room temperature is 22 degrees Celsius. Accurate calculation interval, 5 minutes is selected.

2.6 Heat exchanger model climate

To this end, a fluid heat exchanger was modeled with a constant heat output. The maximum possible heat transfer based on minimum input capacity AWHE fluid was determined.

2.7 Model Water Tank

A mathematical model based on horizontal cylindrical water tank contains a heating coil [8] suggested that we plan to analyze it. Thermal energy balance tank 151 L with 2.5 RSI installed solar house is expressed as follows:

$$m_w\cdot c_{pw}\cdot\frac{dT_w(t)}{dt}=Q_{HE}(t)-U_{tank}\left[T_w(t)-T_o(t)\right] \quad (31)$$

2.8 The model of heat storage in the soil bed

A mathematical model for vertical geothermal reserves in the soil matrix that includes the following assumptions:

The temperature of the soil is ignored, there is a uniform distribution of air flow in crude reserves at 0.2 meters from the seabed soils are divided into five sections. 32-34 In order relations are considered:

$$E_r=Q_{heat}\cdot n \quad (32)$$

$$Vol_r=\frac{E_r}{c_r\rho_r\Delta T} \quad (33)$$

$$A_r=\frac{Vol_r}{H_r} \quad (34)$$

35 The relationship between air temperature and soil surface component as a function of distance and time will tell.

$$-A_r\rho_r c_{pr}\frac{\partial T_r(t)}{\partial t}=\dot{m}_{air}c_{p,air}\frac{\partial T_r(x)}{\partial x}+U_r P(T_r-T_{amb}) \quad (35)$$

Heat transfer rate from the soil bed to heat desired area to cover that area, when air enters the lower part of the bed is out of the soil is determined by the following equation:

$$Q_{supply}=\dot{m}_{air}\cdot c_{p,air}\cdot(T_{r,top}-T_{inlet}) \quad (36)$$

Where the ambient temperature is Tinlet.

3. Experimental arrangements

The first experimental proof configuration model, using data gathered from a variety of devices installed in Solar House Concordia took place. Experimental results are seen in Figure 5. VE Pro software from Agilent was used as a control system and collect data. Air velocity in the BIPV / T at 5 points by speedometer TSI Model 8386A with ± 3% accuracy were measured and the average value was considered as the input operations. Solar Home in the mechanical room, a handmade AWHE Tuesday returns rows with 0.8 installed. T-type thermocouples are used to measure temperature. AWHE wind and water have been installed at both ends. A flow meter with an accuracy of ± 2% in F1000 Polard Electronics Co. AWHE water outlet is located.

4. Additional results and discussion

Outlet air temperature in the cavity configuration under the influence of solar radiation, air velocity and depth of the cavity is located in the cavity. The results are shown in figures 6 and 7. As expected, the recovered heat to produce more severe weather events and therefore are higher energy efficiency. Figure 8 Dependence of heat removal factor FR velocity of air in the cavity, and also shows its depth in the third configuration.

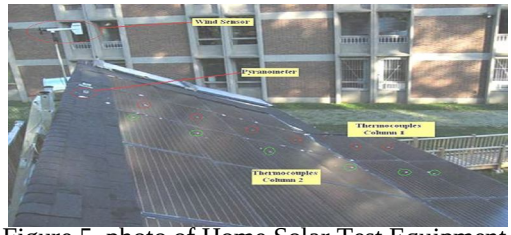

Figure 5. photo of Home Solar Test Equipment.

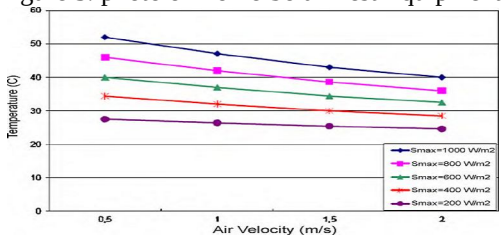

Figure 6. Simulation results of the output air temperature rise in the proportion of solar radiation and air speed changes the configuration of the PV cavity first.

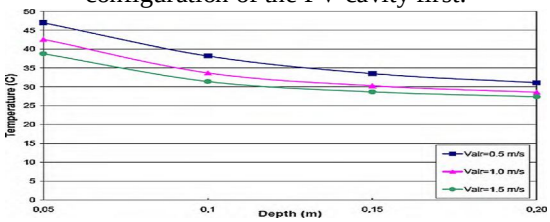

In Figure 7. Simulation output air temperature increases in proportion to the depth of the cavity and the cavity air speed changes the configuration of the first PV.

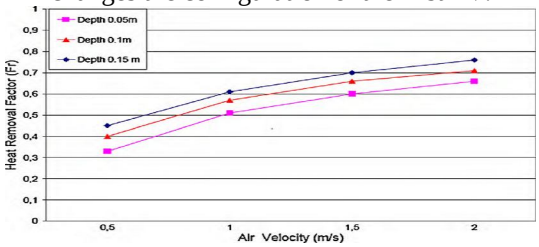

In Figure 8. Heat removal rate is a function of air velocity and depth of the cavity in the third configuration.

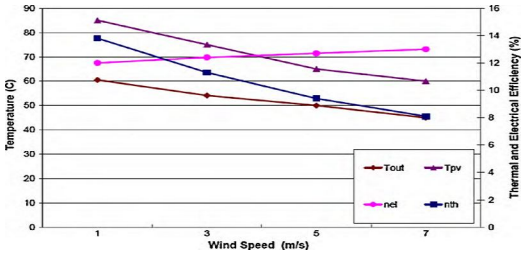

Figure 9. Simulation results with variable speed wind in the first configuration.

Smax=1000 Vair=0.5 To,max=25

PV surface temperature and outgoing air with thermal and electrical performance of the first configuration as a function of wind speed are shown in Figure 9. Following a power law relationship can estimate wind speed with high accuracy [14]

$$\frac{V_z}{V_g} = \left[\frac{Z}{Z_g}\right]^{\Omega} \qquad (37)$$

Average wind speed Vg corresponding decrease in flow velocity in the boundary layer, Zg low altitude, Vz wind speed at any height z above the ground And ΄Ω is the mean speed of 0.1 to 0.4 for the center for sea level changes.

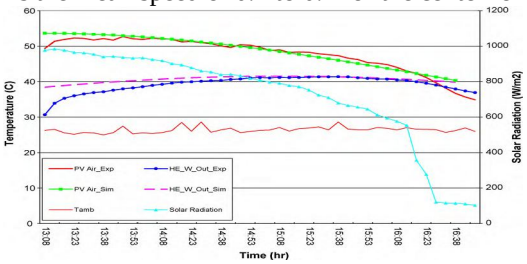

Fig 10. Experimental results and simulated water temperature at the outlet of the first configuration AWHE Smax=985 Vair= 0.4 Vwind= 2.8 To,max= 26

Experimental data and simulated water temperature at the outlet of the first configuration AWHE after time are shown in Figure 10. It can be concluded that the maximum output air temperature glazed roof work BIPV / T at 13:30 was 53 degrees in the afternoon and the sun has started to decrease. The maximum water temperature of 41 degrees is 15:40 AM.

Thermal energy interactions AWHE second and third configuration shown in Figure 11, while the treated water outlet temperature is 42 degrees AWHE second configuration, In the third configuration, the temperature is about 55 degrees Celsius. The initial temperature was set to 12 degrees to the water tank. Simulation results are shown in Figure 12. In the first configuration took approximately 2 hours and 50 minutes at 151 L of water from 12 degrees C to 40 degrees. The configuration of the second and third, respectively, at the same time the water temperature reaches 42 to 55 degrees. A trial date was March days when the wind speed is about 2.2 meters per second and the average temperature on the 2 - level was recorded.

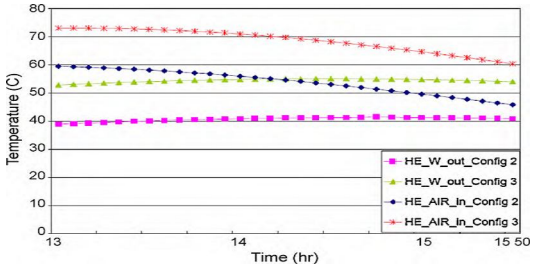

Fig 11. Simulation results of the output water temperature AWHE second configuration Smax = 900 Vair = 0.4 Vwind = 2.8 To, max = 26

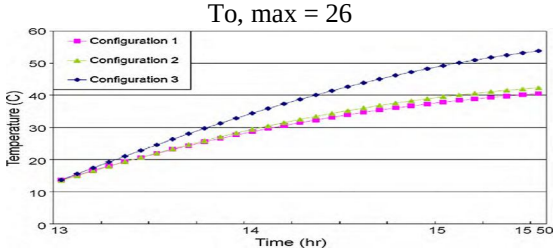

Fig 12. Simulation results AWHE temperature distribution in the heat of the tanker recycled water for all three configurations.

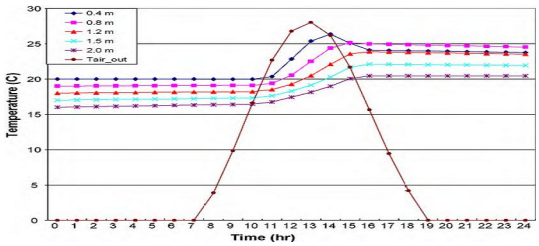

Fig 13. Temperature distribution in soil contexts reserves in the second configuration.

Figure 13 Temperature distribution in the soil substrate stores during the 24-hour period with a steady stream of air into the cavity indicates PV. Surface temperature began to rise at 11:00 and 14:00 h to reach 26 degrees at about 16:00 pm, also started to decrease and reached to 2 degrees Celsius.

After 16:00, the fan was turned off, the temperature of the upper layers of the soil bed were reduced gradually but slowly increased the temperature of the lower layers.

Figure 14 Comparison of heat load before and after the heat supply from the soil bed in the second configuration shows.

Figure 15 also supply air temperature after the heat of the soil bed in the second configuration shows. It can be seen that the temperature has risen above 2.5 degrees Celsius. In order to determine the exact configuration of the energy potential of BIPV / T, electrical and thermal performance in winter and summer, with a maximum number of PV panels and outlet temperature are shown in figures 16 and 17.

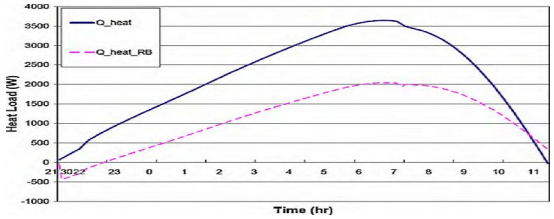

Fig 14. Thermal load of the substrate before and after thermal power configuration in the soil.

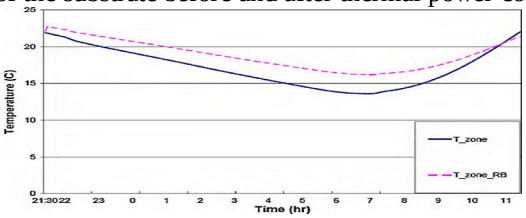

Fig 15. Supply air temperature before and after heating the soil bed in the second configuration.

PV power output of the three configuration types 18 and 19 days compared to typical summer and winter.

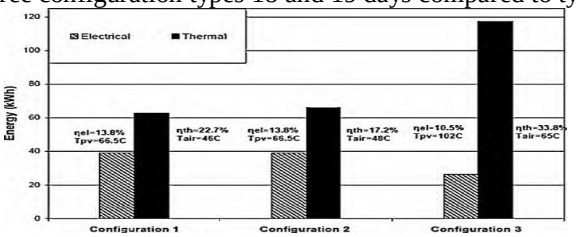

Fig 16. Energy BIPV / T during the summer for all three configurations (thermal and electrical efficiency of the display, the maximum number of PV panels and exhaust air temperatures for all three configurations).

One summer day in the winter, approximately 12.5% more electricity is produced.

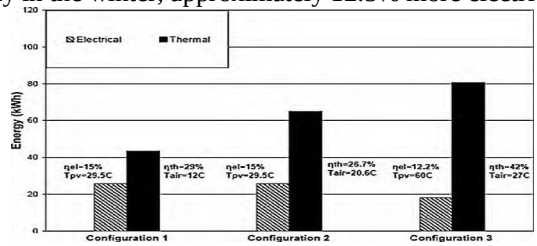

Fig 17. Energy BIPV / T for the three configurations on a winter day.

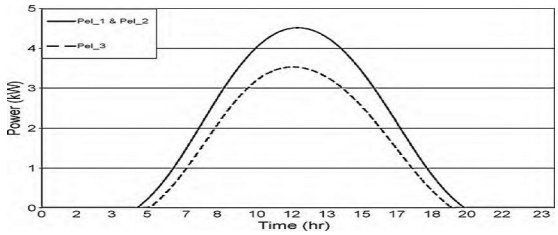

Fig 18. PV power output configurations first, second and third day 17 July.

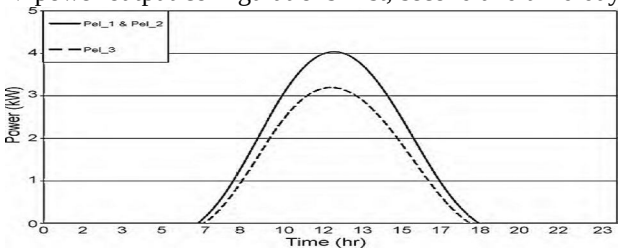

Fig 19. PV power output configurations first, second and third on the 16th day of February.

5. Conclusions

In this article three different heating systems. Vltayy photovoltaic open circuit inside the building embedded in the ceiling with their artificial systems, heat recovery and utilization of heat to raise the thermal efficiency was compared And three BIPV / T Bartndazsqf the BIPV / T do not mucilage Vsqf BIPV / T not working with a glazed roof that collects and finally glazed BIPV / T glazing work Several mathematical models were introduced for all configurations and the relative were compared.

The second and third can be configured in order to significantly increase thermal efficiency and output air temperatures used. Instead, the third configuration reduces electricity and may lead to excessive temperature rise in the PV panels. System BIPV / T do not mucilage is suitable for placement in a bed of soil in winter will generate more heat energy. Finally, it is necessary to add that the air in open systems BIPV / T can be then used to filter the air.

REFERENCES

[1] R. Charron, A. Athienitis, Optimization of the performance of double-facades with integrated photovoltaic panels and motorized blinds, Solar Energy 80 (2006) 482–491.

[2] M. Bakker, H. Zondag, M. Elswijk, K. Strootman, M. Jong, Performance and costs of a roof-sized PV/thermal array combined with a ground coupled heat pump, Solar Energy 78 (2005) 331–339.

[3] M. Mottillo, I. Beausoleil-Morrison, L. Couture, Y. Poissant, A Comparison and Validation of 2 Photovoltaic Models, Canmet Energy, NRCAN, Canada, Visited: December 15th, http://canmetenergy-canmetenergie.nrcan-rncan.gc.ca, 2009.

[4] J. Ji, J. Han, T. Chow, H. Yi, J. Lu, W. He, W. Sun, Effect of fluid flow and parking factor on energy performance of a wall-mounted hybrid photovoltaic/waterheating collector system, Energy and Buildings 38 (2006) 1380–1387.

[5] J.A. Candanedo, B. O'Neill, S. Pantic, A. Athienitis, Studies of control strategies for the Concordia solar house, in: Proceedings of the 2nd Canadian Solar Buildings Conference, Calgary, Canada, 2007.

[6] Y. Chen, A.K. Athienitis, K.E. Galal, Y. Poissant, Design and simulation for a solar house with building integrated photovoltaic-thermal system and thermal storage, in: Proceedings of the ISES Solar World Congress, vol. I, Beijing, China, 2007, pp. 327–332.

[7] MathCAD Professional 2001i, Mathsoft Engineering & Education Inc., Cambridge, MA, USA, 2001.

[8] J. Duffie, W. Beckman, Solar Engineering of Thermal Processes, 2nd ed., John Wiley & Sons, New York, USA, 1980.

[9] F. Incropera, D. DeWitt, Fundamentals of Heat and Mass transfer, 2nd edition, John Wiley & Sons, New York, USA, 1985.

[10] K. Ong, Thermal performance of solar air heaters: mathematical model and solution procedure, Solar Energy 55 (2) (1995) 93–109.

[11] V. Gnielinski, Forced Convection in Ducts, Hemisphere Publishing Corporation, 1983.

[12] A. Athienitis, M. Santamouris, Thermal Analysis and Design of Passive Solar Buildings, James & James Ltd., London, UK, 2002.

[13] Agilent VEE Pro 8.0, Agilent Technologies Inc., Santa Clara, CA, USA, 2006.

[14] N. Hutcheon, G. Handegord, Building Science for a Cold Climate, National Research Council of Canada, 1995.